Investigating Antibody Interactions with a Polar Liquid Using Terahertz Pulsed Spectroscopy

Yiwen Sun,[†] Yuanting Zhang,[†] and Emma Pickwell-MacPherson[‡*]
[†]Department of Electronic Engineering, The Chinese University of Hong Kong, Shatin, Hong Kong; and [‡]Department of Electronic and Computer Engineering, The Hong Kong University of Science and Technology, Clearwater Bay, Hong Kong

ABSTRACT In this article, we use terahertz spectroscopy to study the dielectric properties of the peroxidase-conjugated affinity purified goat anti-cat immunoglobulin G and the fluorescein-conjugated affinity purified goat anti-cat immunoglobulin G when they interact with polar liquids. The influence of protein concentration, as well as presence of glycerol as a cosolvent, is determined by estimation of the effective hydration shell radius of the protein in solution. The dielectric spectra in this study are measured over the frequency range 0.1–1.3 THz and it is found that the dielectric properties are dependent on the type of the charges in the hydrogen-bonded antibodies' networks. Our results indicate that the terahertz dielectric properties of polar liquids are strongly affected by the presence of the antibody and suggest that the dielectric spectrum is particularly powerful in the study of structural and conformational properties of proteins. Therefore, terahertz spectroscopy is a very sensitive approach to investigate structural features of biological systems.

INTRODUCTION

Proteins influence both the spatial and dynamic arrangement of neighboring liquid layers through weak intermolecular interactions (1). The collective vibrational modes are associated with the protein's tertiary structure and lie in the far infrared or terahertz (THz) frequency range (2–4). These modes are due to intermolecular interactions and can be probed in crystalline molecules (which may contain bound water) in their solid form as well as in solution. For example, THz spectroscopy has been used to study the transformation of the α-helix into a β-sheet during insulin amyloid fibrillation (5). Glycerol has been used for many years as one of the common solvent additives to stabilize the activity of enzymes and the native structure (folded state) of proteins.

With the advent of pulsed THz techniques, low frequency dielectric characterization of proteins can be accomplished. Dielectric spectroscopy is a noninvasive, very sensitive technique to investigate complex biological water systems as detailed in previous reviews (6–8). The far-infrared dielectric properties are dominated by vibrational modes of the intermolecular hydrogen-bonded network (9). Indeed, the dielectric spectrum can be used to investigate a number of diverse biological phenomena such as cell division in lower eukaryotes, ion transport across the membrane, and impact of different types of stress on cells as well as cell aging (10–13). There is abundant literature on the investigation of biological systems such as globular β-lactoglobulin, hen egg white lysozyme, and short-chain peptide in solid-phase using THz spectroscopy (14–16). However, labeled immunoglobulin G (IgG), which constitutes an extremely interesting and ample field of research, has not been as intensely studied by this technique. In this article, we conduct THz spectroscopy to study the behavior of antibodies in polar liquid solutions.

Elevated levels of different classes of immunoglobulins can often be used to determine the cause of liver damage in patients for whom the diagnosis is unclear (17). Immunoglobulin G is the most abundant class of antibodies found in blood and tissue liquids and is especially elevated in viral hepatitis, autoimmune hepatitis, and cirrhosis (18). Therefore, overexpression of specific IgGs could serve as a biomarker for rapid diagnosis of both acute and persistent infections. Thus, we investigate whether the THz properties of biological liquids are affected by the presence of a specific IgG to determine whether THz spectroscopy could potentially be used for antibody detection in the future.

MATERIALS AND METHODS

Two types of antibodies are selected for this investigation. The peroxidase (PX)-conjugated affinity purified goat anti-cat IgG powder and the fluorescein (FITC)-conjugated affinity purified goat anti-cat IgG powder (Jackson ImmunoResearch Laboratories, West Grove, PA) are mixed with a 50/50 solution of distilled water and glycerol (L6876; Sigma-Aldrich, St. Louis, MO) to obtain a protein concentration of 0.8 mg/mL, and stored in the dark below 4°C. Glycerol is a common component of solvents dissolved in water as it stabilizes the protein molecules and, for frozen samples, it reduces damage due to ice crystal formation. Because the proteins are stored in a 50/50 glycerol/water solution, 50/50 glycerol/water was used to dilute original solution to obtain concentrations of 0.56, 0.4, 0.27, and 0.16 mg/mL. The solutions at room temperature are clear and without precipitates.

The measurements are performed in reflection geometry using a modified version of the TPI Imaga 1000 (TeraView, Cambridge, UK) to obtain the data. A similar optical set up has been described by Pickwell et al. (19). Briefly, the system uses photoconductive antennas for generation and detection of THz radiation, and an ultrafast laser (Vitesse; Coherent, Santa Clara, CA) emits 90 fs pulses centered at a wavelength of 800 nm, with a 80 MHz

Submitted April 15, 2010, and accepted for publication November 16, 2010.

*Correspondence: eeemma@ust.hk

Yiwen Sun's present address is Medical School, Shenzhen University, Guangdong, 518060, People's Republic of China.

Editor: Feng Gai.

0006-3495/11/01/0225/7 $2.00

doi: 10.1016/j.bpj.2010.11.020

repetition rate and an average power of ~200 mW. The laser beam is separated into the pump and probe beams by a beam splitter, but in contrast to the TPI Imaga 1000 (TeraView), the laser in this system used for optical excitation reaches the antennas via a fiber optic, rather than through free space optics. The quartz window on the probe head is used to contact the liquid sample directly with an angle of incidence of 3.4° and the reflected terahertz pulse from the quartz/sample interface is detected coherently. The pulse incident on the lower surface of the quartz is separated from the pulse reflected off the sample by ~10 ps.

To account for any enduring wave effects from the lower surface we measured a baseline, as detailed in Huang et al. (20), and subtracted this from our sample and reference measurements. The terahertz wave can penetrate the sample by ~500 μm. Therefore, to avoid unwanted reflections in the sample, we prepared a liquid layer which is of the order of a few millimeters thick. The usable frequency range is from ~0.1 THz to 1.6 THz, but the valid range tends to decrease when the sample is in an aqueous phase due to signal attenuation by the sample.

THz spectroscopy is typically done with a single point measurement of a homogenous sample and the resulting THz electric field can be recorded as a function of time. In this study, the complex refractive index can be acquired through consideration of Fresnel's coefficient in a reflection geometry. The incident and the reflected electric fields are determined by the Fresnel's equations as well as their polarization statuses (21).

A fast Fourier transform of the temporal profiles was performed to offer meaningful spectroscopic information due to the broadband nature of pulsed THz radiation. We used a measurement of air as a reference. Because the incident THz light is s-polarized in our system, the complex spectrum $E_{ref}(\omega)$ of the reference THz pulse is related to the complex spectrum

$$E_{sam}(\omega)$$

of the output THz pulse by Eq. 1, where

$$k(\omega) = n(\omega)\omega/c - (\alpha(\omega)/2)i$$

and $n(\omega)$ is the frequency-dependent refractive index, $\alpha(\omega)$ is the frequency-dependent absorption coefficient, and c is the speed of light in a vacuum,

$$\begin{aligned} R &= \frac{E_{sam}(\omega)}{E_{ref}(\omega)} \\ &= \frac{k_{quartz}(\omega)\cos\theta_{quartz} - k_{sam}(\omega)\cos\theta_{sam}}{k_{quartz}(\omega)\cos\theta_{quartz} + k_{sam}(\omega)\cos\theta_{sam}} \\ &\quad \times \frac{k_{quartz}(\omega)\cos\theta_{quartz} + k_{air}(\omega)\cos\theta_{air}}{k_{quartz}(\omega)\cos\theta_{quartz} - k_{air}(\omega)\cos\theta_{air}}. \end{aligned} \tag{1}$$

To extract k_{sam}, we rearrange above equation as below,

$$k_{sam}\cos\theta_{sam} = \frac{(1-R)k_{quartz}^2\cos^2\theta_{quartz} + (1+R)k_{quartz}\cos\theta_{quartz}k_{air}\cos\theta_{air}}{(1-R)k_{air}\cos\theta_{air} + (1+R)k_{quartz}\cos\theta_{quartz}}. \tag{2}$$

From Snell's law, we know that the angle is actually dependent on the refractive index of the medium where the light propagates,

$$n_{sam}\sin\theta_{sam} = n_{air}\sin\theta_{air}. \tag{3}$$

By rearranging Eq. 2, we also know that

$$n_{sam}\cos\theta_{sam} = \frac{c}{\omega}\mathrm{Re}\left\{k_{quartz}\cos\theta_{quartz}\frac{(1-R)k_{quartz}\cos\theta_{quartz} + (1+R)k_{air}\cos\theta_{air}}{(1-R)k_{air}\cos\theta_{air} + (1+R)k_{quartz}\cos\theta_{quartz}}\right\}. \tag{4}$$

Then by solving Eq. 3 and Eq. 4 simultaneously, we can obtain $\cos\theta_{sam}$. This can then be used in the equations below for the refractive index and absorption coefficient which come directly from the real and imaginary parts of Eq. 2:

$$n(\omega) = \frac{c}{\omega\cos\theta_{sam}}\mathrm{Re}\left\{k_{quartz}\cos\theta_{quartz}\frac{(1-R)k_{quartz}\cos\theta_{quartz} + (1+R)k_{air}\cos\theta_{air}}{(1-R)k_{air}\cos\theta_{air} + (1+R)k_{quartz}\cos\theta_{quartz}}\right\}, \tag{5}$$

$$\alpha(\omega) = -\frac{2}{\cos\theta_{sam}}\mathrm{Im}\left\{k_{quartz}\cos\theta_{quartz}\frac{(1-R)k_{quartz}\cos\theta_{quartz} + (1+R)k_{air}\cos\theta_{air}}{(1-R)k_{air}\cos\theta_{air} + (1+R)k_{quartz}\cos\theta_{quartz}}\right\}. \tag{6}$$

RESULTS AND DISCUSSION

Terahertz dielectric properties

The complex permittivity ε^* is expressed by the real part ε' and the imaginary part ε'' ($\varepsilon^* = \varepsilon' - i\,\varepsilon''$) in which the real part corresponds to the dielectric constant and the imaginary part, known as the dielectric loss factor, is a measure of the energy absorption per cycle (1). We extracted the dielectric constant and the dielectric loss spectrum of the protein solutions to indicate the effects of these two antibodies. The real and imaginary parts of the complex permittivity were calculated from the frequency-dependent optical constants $n(\omega)$ and $\alpha(\omega)$ as detailed in Eq. 7, and are plotted in Fig. 1 for the 50/50 water/glycerol mix, peroxidase-conjugated IgG (PX-IgG), and the fluorescein conjugated IgG (FITC-IgG),

$$\begin{aligned} \varepsilon^* &= \left(n(\omega) - i\left(\tfrac{c\alpha(\omega)}{2\omega}\right)\right)^2 \\ &= n(\omega)^2 - \left(\tfrac{c\alpha(\omega)}{2\omega}\right)^2 - 2n(\omega)\left(\tfrac{c\alpha(\omega)}{2\omega}\right)i \\ &= \varepsilon' - i\varepsilon'' \\ \Rightarrow \varepsilon' &= n(\omega)^2 - \left(\tfrac{c\alpha(\omega)}{2\omega}\right)^2 \\ \Rightarrow \varepsilon'' &= 2n(\omega)\left(\tfrac{c\alpha(\omega)}{2\omega}\right). \end{aligned} \tag{7}$$

In Fig. 1 *A*, compared to the solvent, PX-IgG has a higher dielectric constant than FITC-IgG over the whole frequency range. There are two noticeable peaks in the dielectric loss spectrum of PX-IgG at 0.76 and 1.18 THz.

The dielectric loss factor $\varepsilon''(\omega)$, is of particular interest in this work, because it is related by the general fluctuation-dissipation theorem to the spectrum of polarization

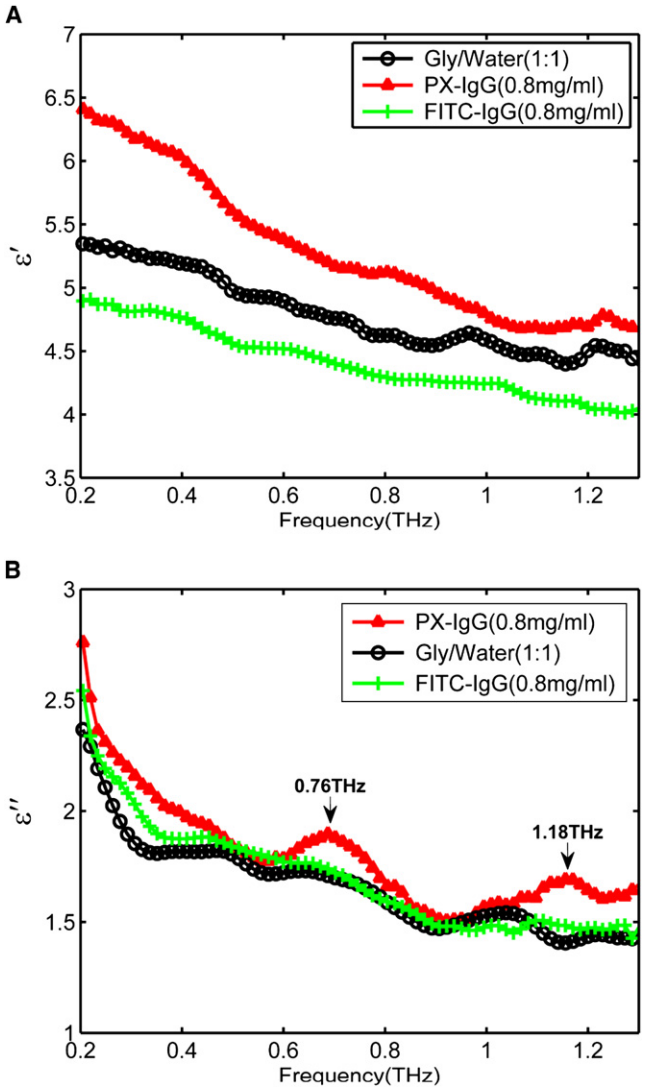

FIGURE 1 (*A*) Dielectric constant spectra and (*B*) dielectric loss spectra of water/glycerol mix (*black line* with *circles*), peroxidase-conjugated IgG (PX-IgG) (*red line* with *triangles*), and the fluorescein-conjugated IgG (FITC-IgG) (*green line* with *crosses*) dissolved in the water/glycerol solution at a concentration of 0.8 mg/mL. Error bars for the 95% confidence intervals are too small to be seen when plotted.

fluctuations of a dielectric sample that originate from thermally induced translational stochastic motions of charge carriers and the rotational tumbling motion of dipolar entities. Furthermore, due to the relative broadness of the dielectric spectra, the different relaxation processes will only be resolved adequately if the polar molecules under investigation differ significantly in size (22). This is the case for the ternary glycerol-water-protein system studied here. The low frequency contribution to relaxation can be assigned unambiguously to the motion of the protein whereas the high frequency contributions result from the solvent (22).

In Fig. 1 *B*, we observe that the glycerol-water solvent provides a noticeable loss contribution in the low frequency region (from 0.2 to 0.4 THz). There are also underlying oscillations present in the solvent and both antibody solutions: we attribute these oscillations to the solvent. However, PX-IgG (*red line* with *triangles*) has significantly higher contributions centered at 0.76 THz and 1.18 THz. These vibrational modes are most likely to be due to the weak intermolecular interactions between the peroxidase and the IgG. The spectra of the solvent (*black line* with *circles*) and FITC-IgG (*green line* with *crosses*) do not show any clear band structure; they only decrease monotonically with frequency. See also Table 1.

It is known that the effect of the dynamic depolarization, which is proportional to the solution conductivity, depends only on the dielectric properties of the solution (23). A charge that moves in the driving electric field (the THz pulse) causes the surrounding solvent molecules to rotate (24). The direction of this rotation has an opposite sign compared to the direction of the electric field, hence resulting in a decrease in the dielectric relaxation strength. It is reported that IgG fractions are negatively charged and that addition of fluorescein renders them more electronegative (25), whereas in the studies of Herrmann et al. (26), they found by gel electrophoresis that peroxidase has a positive charge. Hence, due to the type of the charges in the hydrogen-bonded antibodies networks, dielectric spectra indicate the difference between antibody PX-IgG and FITC-IgG. Furthermore, positively charged PX-IgG aqueous networks significantly enhance the dielectric relaxation strength.

Dielectric spectra consist of many bands originating from vibrational modes (27). The only differences between the molecular structures for the two antibodies are in the conjugation pattern, whether it is peroxidase- or fluorescein-conjugated. FITC is the fluorescein base molecule functionalized with an isothiocyanate reactive group (–N=C=S) at one of two hydrogen atoms on the bottom ring of the structure. This derivative is covalently coupled to primary amine groups on proteins of the immunoglobulin, whereas sugar residues present on peroxidase can be oxidized to produce aldehydes which react with primary amines on antibodies (28).

The conjugation scheme for the FITC and peroxidase reaction with an amine on immunoglobulin is shown in Fig. 2. As we see from Fig. 2, the PX-IgG contains a reactive aldehyde group but the FITC-IgG does not, thus it is likely that this group is responsible for the strong absorption. Previous studies of α-lactose monohydrate (which also contains an aldehyde group) support this hypothesis, because two absorption peaks at similar frequencies (0.52 and 1.38 THz) were also observed at room temperature (29). It would be interesting to see how and if the absorption features change when a substrate is bound to the antibodies, but this lies beyond the scope of this study.

TABLE 1 Comparison of average molecular mass (MM), average antibody radius (AR), and depth of hydration shell (DHS) of PX-IgG and FITC-IgG

	MM (KDa)	AR (Å)	DHS (Å)
PX-IgG	210	53.4 ± 3.3	17.7 ± 3.3
FITC-IgG	152	48.0 ± 1.5	23.1 ± 1.5

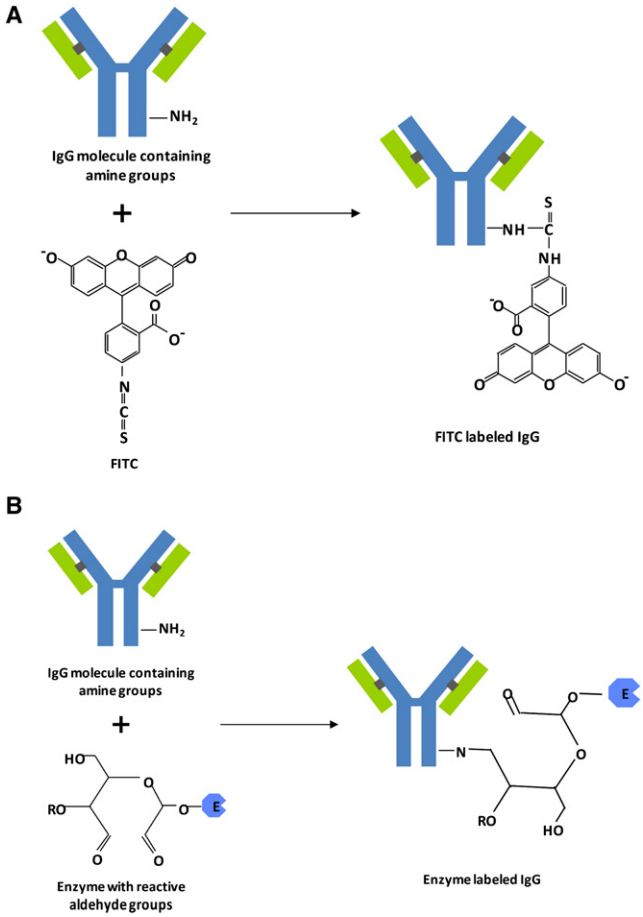

FIGURE 2 Conjugation scheme for (*A*) FITC and (*B*) enzyme reaction with a primary amine on immunoglobulin.

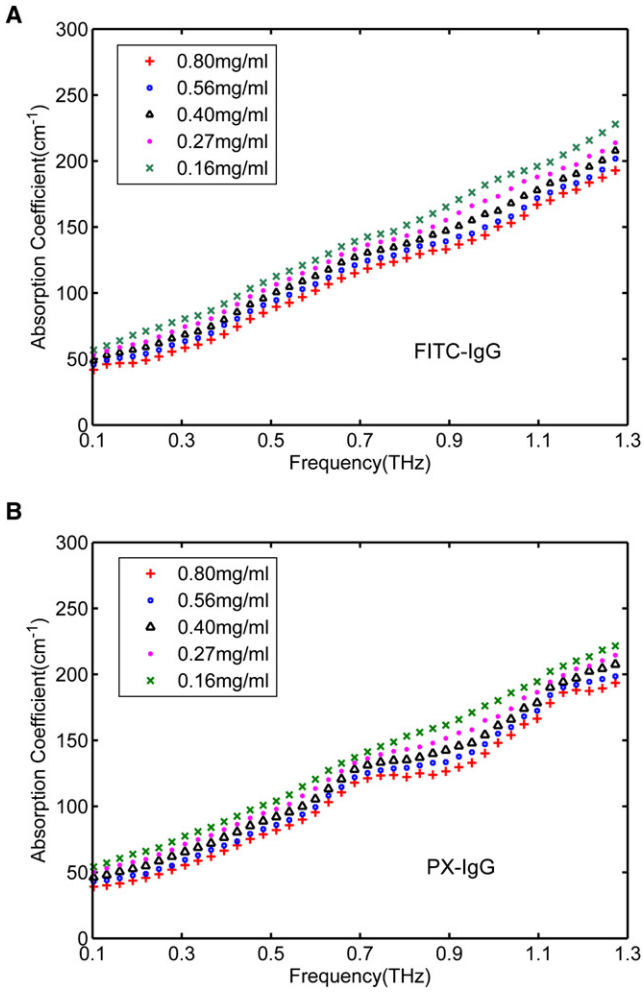

FIGURE 3 Absorption coefficients of (*A*) FITC-IgG and (*B*) PX-IgG in 50% glycerol solution at concentrations: 0.16, 0.27, 0.4, 0.56, and 0.8 mg/mL (*red solid line*). Error bars for the 95% confidence intervals are too small to be seen when plotted.

Concentration-dependent measurements

Fig. 3 shows the dependence of the absorption coefficients on the concentration of the antibodies PX-IgG and FITC-IgG. THz absorption spectra are very sensitive to crystalline structures (30,31), but the liquid protein form of FITC-IgG lacked any distinct peaks in the spectral region studied. However, the PX-IgG exhibited spectral peaks at 0.76 and 1.18 THz approximately (i.e., at the same location as the absorption peaks in Fig. 1 *B*). As expected, these peaks became submerged as the protein concentration was decreased. The absolute overall absorption increases with decreasing protein fraction, because THz is absorbed strongly by the water in the solvent. When we compare the absorbance of two antibody proteins at the same frequency, the absorbance of FITC-IgG is consistently higher than that of PX-IgG.

We determined the THz absorption coefficient $\alpha_{ideal}(\omega)$ as a linear function of increasing protein concentration in the solvent volume *V*. We expect the proteins to be much less absorbing than the glycerol solution and so expect the absorption coefficient to decrease with increasing protein concentration. In Fig. 4, the THz absorption at various concentrations of antibodies FITC-IgG (*green marks*) and PX-IgG (*red marks*) in 50% glycerol solutions is determined at 0.45 THz. We used Eq. 8 (32) for the absorption coefficient of an ideal mixture. Equation 8 is based on the two-component excluded volume model and was used to fit absorption coefficient versus protein concentration,

$$\alpha_{ideal}(\omega) = A_1\alpha_{protein}(\omega) + A_2\alpha_{solvent}(\omega), \qquad (8)$$

where α_i is the absorption coefficient for each component, and the coefficient

$$A_1 = V_{\text{protein}}/V \text{ and } A_2 = \left(V - V_{\text{protein}}\right)/V.$$

THz absorption decreases linearly with the protein concentration increasing from 0.16 to 0.56 mg/mL and then deviates at the higher protein concentration as shown in Fig. 4. Such a nonmonotonic, nonlinear behavior cannot be explained simply by a two-component excluded volume model. The water layer around the protein molecule is known to exhibit distinct dynamical properties compared

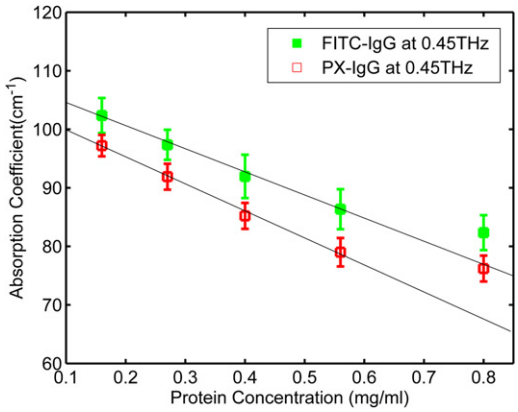

FIGURE 4 Terahertz absorption of antibodies in 50% glycerol solutions at 0.45 THz. The line with solid green squares represents the fluorescein conjugated IgG (FITC-IgG) and the line with red hollow squares represents the peroxidase conjugated IgG (PX-IgG). The lines are fitted to highlight the linear behavior when the concentration changed from 0.16 to 0.56 mg/ml. The error bars are the 95% confidence intervals.

with bulk water. In Fig. 4, the nonlinear change can be explained as the beginning of overlap of the dynamical hydration shell around the protein molecule.

Therefore, we continued our analysis in terms of individually determined absorption coefficients using a ternary component model (protein, hydration water, and bulk water), which assumes a distinct absorption coefficient of the water around the solute molecule due to the distinct properties of the solvation water (33). In this model expressed by Eq. 9, the ideal absorption coefficient is described as the volume-weighted fraction of the absorption of the protein, the hydration water, and the bulk water,

$$\alpha_{ideal}(\omega) = A_1\alpha_{protein}(\omega) + A_2\alpha_{hydration\_shell}(\omega) + A_3\alpha_{bulk\_water}(\omega). \quad (9)$$

IgG antibodies are large molecules of ~150 kDa composed of four peptide chains. Typically they contain two identical heavy chains of ~50 kDa and two identical light chains of ~25 kDa. The enzyme (e.g., peroxidase) and the fluorophore (e.g., fluorescein) can be tagged on the IgG to become a labeled antibody (34). The number of tagged molecules per antibody affects the overall conformation of the combined molecule. In our study there are 1–2 peroxidase molecules (molecular mass: 40 kDa) per IgG molecule and 4–7 fluorescein molecules (molecular mass: 390 Da) per IgG molecule (35). We assume that the tagged antibody is a homogenous hard sphere. This is appropriate because we are probing the properties at a macroscopic level: consequently, the molecular orientation distribution is assumed to be random across the sample, resulting in an isotropic average molecular conformation.

Using a classic method (36), the effective hydrodynamic radius R_b for a bare IgG molecule is

$$R_b = 55.1 \pm 0.3 \text{ Å}.$$

The radius of the hydrated IgG molecule, R_0, is given by (33)

$$R_0 = R_b \cdot \sqrt{(5/3)}.$$

This is 71.1 ± 0.4 Å for the IgG molecule. From Fig. 4 we see that the absorption coefficient starts to behave nonlinearly above a concentration of 0.56 mg/mL—this is due to hydration shell overlap. From the graph, we deduce that the nonlinear behavior started between concentrations 0.5 mg/mL and 0.6 mg/mL. We therefore use these concentrations for $c_{protein}$ in the formula below to determine limits for the average radius R of the antibody molecule,

$$\frac{4\pi}{3}R^3 = \frac{m_{mass}}{c_{protein}N_A}, \quad (10)$$

where m_{mass} is the molecular mass and N_A is the Avogadro constant. The molecular mass of the tagged antibody depends on the number of tagged molecules per IgG molecule, so to determine the upper and lower limits of the radius we also need to consider the highest and lowest possible molecular masses in conjunction with the lowest and highest concentrations for $c_{protein}$. These give limits on the average radius for PX-IgG of 50.1 Å to 56.7 Å so that

$$R = 53.4 \pm 3.3 \text{ Å}.$$

Similarly, the average radius for FITC-IgG is

$$R = 48.0 \pm 1.5 \text{ Å}.$$

From these we can directly deduce the thickness of the hydration shell ($R_{shell} = R_0 - R$) to be

$$17.7 \pm 3.3 \text{ Å}$$

for PX-IgG and

$$23.1 \pm 1.5 \text{ Å}$$

for FITC-IgG. It has been found that the binding of native antibodies causes a decrease in the radius (R_b) of up to 2 Å for PX-IgG and 7 Å for FITC-IgG (37) and so our calculations of hydration shell thicknesses are maximum values. The above discussion is shown schematically in Fig. 5. Similar values of the hydration shell have been reported by Heugen et al. (38). As the concentration of the antibodies increases, the hydration shells start to overlap and result in nonlinear absorption. Eventually, the hydration shells overlap fully and are saturated such that it is not possible to increase the concentration further. This occurs at much higher concentrations than those which we investigated in this study. A greater variety of concentrations would ideally be investigated in further work.

SUMMARY

In this study, we have determined the effects of two antibodies on the dielectric properties of a polar liquid from

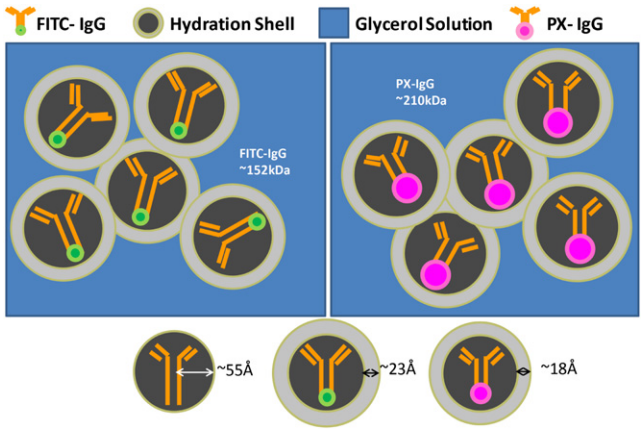

FIGURE 5 Schematic diagram for overlap of the hydration shells for FITC-IgG and PX-IgG in the glycerol solution.

0.1 to 1.3 THz. The complex permittivity response of the polar liquid and the proteins in solution have been measured as a function of frequency. The response is strongly associated with the polarization arising from the polar liquids' network of hydrogen bonding. The presence of different antibodies affected the solution uniquely such that the dielectric properties of each solution containing an antibody were sensitive to the conjugation of the antibody added. This highlights that hydrogen-bonded networks of charged protein solutions play an important role in determining the dielectric properties detected by THz spectroscopy.

In further work, we will also investigate different dielectric relaxation models of liquids and the distribution function for more complex protein-liquid systems, so as to understand and relate the measurements to the molecular changes occurring.

The authors thank Dr. K. Qin (Department of Microbiology, The University of Hong Kong, Hong Kong) for guidance of sample preparation.

We gratefully acknowledge partial financial support for this work from the Research Grants Council of the Hong Kong Government and the Shun Hing Institute of Advanced Engineering, Hong Kong.

REFERENCES

1. Pethig, R. 1992. Protein-water interactions determined by dielectric methods. *Annu. Rev. Phys. Chem.* 43:177–205.
2. Markelz, A., A. Roitberg, and E. J. Heilweil. 2000. Pulsed terahertz spectroscopy of DNA, bovine serum albumin and collagen between 0.06 to 2.00 THz. *Chem. Phys. Lett.* 320:42–48.
3. Markelz, A., S. Whitmire, …, R. Birge. 2002. THz time domain spectroscopy of biomolecular conformational modes. *Phys. Med. Biol.* 47:3797–3805.
4. Fischer, B. M., M. Walther, and P. Uhd Jepsen. 2002. Far-infrared vibrational modes of DNA components studied by terahertz time-domain spectroscopy. *Phys. Med. Biol.* 47:3807–3814.
5. Liu, R., M. X. He, …, Z. He. 2010. Insulin amyloid fibrillation studied by terahertz spectroscopy and other biophysical methods. *Biochem. Biophys. Res. Commun.* 391:862–867.
6. Yardley, J. E., D. B. Kell, …, C. L. Davey. 2000. On-line, real-time measurements of cellular biomass using dielectric spectroscopy. *Biotechnol. Genet. Eng. Rev.* 17:3–35.
7. Schuster, K. C. 2000. Monitoring the physiological status in bioprocesses on the cellular level. *Adv. Biochem. Eng. Biotechnol.* 66: 185–208.
8. Asami, K. 2002. Characterization of heterogeneous systems by dielectric spectroscopy. *Prog. Polym. Sci.* 27:1617–1659.
9. Walther, M., B. M. Fischer, and P. U. Jepsen. 2003. Noncovalent intermolecular forces in polycrystalline and amorphous saccharides in the far infrared. *Chem. Phys.* 288:261–268.
10. Pedone, F., and A. Bonincontro. 1991. Temperature dependence of DNA dielectric dispersion at radiofrequency. *Biochim. Biophys. Acta.* 1073:580–584.
11. Laudat, J., and F. Laudat. 1992. Dielectric study of charge motion in DNA. *Eur. Biophys. J.* 21:233–239.
12. Degouys, V., I. Cerckel, …, A. O. Miller. 1993. Dielectric spectroscopy of mammalian cells. 2. Simultaneous in situ evaluation by aperture impedance pulse spectroscopy and low frequency dielectric spectroscopy of the biomass of HTC cells on Cytodex 3. *Cytotechnology.* 13:195–202.
13. Bonincontro, A., G. Melucci-Vigo, and G. Risuleo. 1993. Mouse polyomavirus mediated effects on the infected cell membrane studied by dielectric spectroscopy. *Biosci. Rep.* 13:259–263.
14. Png, G. M., R. J. Falconer, …, D. Abbott. 2009. Terahertz spectroscopic differentiation of microstructures in protein gels. *Opt. Express.* 17:13102–13115.
15. Kutteruf, M. R., C. M. Brown, …, E. J. Heilweil. 2003. Terahertz spectroscopy of short-chain polypeptides. *Chem. Phys. Lett.* 375:337–343.
16. Knab, J., J. Y. Chen, and A. Markelz. 2006. Hydration dependence of conformational dielectric relaxation of lysozyme. *Biophys. J.* 90: 2576–2581.
17. Rhoades, R. A., and R. G. Pflanzer. 2002. Human Physiology, 4th Ed. Thomson Learning, Pacific Grove, CA.
18. Boberg, K. M., E. Aadland, …, H. Bell. 1998. Incidence and prevalence of primary biliary cirrhosis, primary sclerosing cholangitis, and autoimmune hepatitis in a Norwegian population. *Scand. J. Gastroenterol.* 33:99–103.
19. Pickwell, E., B. E. Cole, …, V. P. Wallace. 2004. In vivo study of human skin using pulsed terahertz radiation. *Phys. Med. Biol.* 49:1595–1607.
20. Huang, S. Y., P. C. Ashworth, …, E. Pickwell-MacPherson. 2009. Improved sample characterization in terahertz reflection imaging and spectroscopy. *Opt. Express.* 17:3848–3854.
21. Jepsen, P. U., U. Møller, and H. Merbold. 2007. Investigation of aqueous alcohol and sugar solutions with reflection terahertz time-domain spectroscopy. *Opt. Express.* 15:14717–14737.
22. Betting, H., M. Hackel, …, M. Stockhausen. 2001. Spectroscopic evidence for the referential hydration of RNase A in glycerol. water mixtures: dielectric relaxation studies. *Phys. Chem. Chem. Phys.* 3:1688–1692.
23. Buchner, R., G. T. Hefter, and P. M. May. 1999. Dielectric relaxation of aqueous NaCl solutions. *J. Phys. Chem. A.* 103:1–9.
24. Hubbard, J. B., L. Onsager, …, M. Mandel. 1977. Kinetic polarization deficiency in electrolyte solutions. *Proc. Natl. Acad. Sci. USA.* 74: 401–404.
25. Mellors, R. C. 1968. The application of labeled antibody technics in studying cell antigens. *Cancer Res.* 28:1372–1381.
26. Herrmann, J. E., S. A. Morse, and M. F. Collins. 1974. Comparison of techniques and immunoreagents used for indirect immunofluorescence and immunoperoxidase identification of enteroviruses. *Infect. Immun.* 10:220–226.
27. Levitt, M., C. Sander, and P. S. Stern. 1985. Protein normal-mode dynamics: trypsin inhibitor, crambin, ribonuclease and lysozyme. *J. Mol. Biol.* 181:423–447.
28. Pierce Protein Research Products. Thermo Scientific. http://www.piercenet.com.

29. Parrott, E. P., J. A. Zeitler, and L. F. Gladden. 2009. Accurate determination of optical coefficients from chemical samples using terahertz time-domain spectroscopy and effective medium theory. *Opt. Lett.* 34:3722–3724.

30. Taday, P. F., I. V. Bradley, and D. D. Arnone. 2003. Terahertz pulse spectroscopy of biological materials: L-glutamic acid. *J. Biol. Phys.* 29:109–115.

31. Taday, P. F., I. V. Bradley, …, M. Pepper. 2003. Using Terahertz pulse spectroscopy to study the crystalline structure of a drug: a case study of the polymorphs of ranitidine hydrochloride. *J. Pharm. Sci.* 92:831–838.

32. Tassaing, T., Y. Danten, …, J. Yarwood. 1994. A far infrared study of benzene-fluorinated benzene binary mixtures. *Chem. Phys.* 184: 225–231.

33. Seung, J. K. 2008. Studies of protein-protein and protein-water interactions by small angle x-ray scattering, terahertz spectroscopy, asmos, and computer simulation. PhD Thesis. University of Illinois at Urbana-Champaign, Champaign, IL.

34. Campbell, A. M. 1984. Monoclonal Antibody Technology. Elsevier Science Publishers, Dordrecht, The Netherlands.

35. Reilly, J. T. 1996. Use and evaluation of leukocyte monoclonal antibodies in the diagnostic laboratory: a review. *Clin. Lab. Haematol.* 18:1–5.

36. Pino, R. M., and C. L. Thouron. 1983. Vascular permeability in the rat eye to endogenous albumin and immunoglobulin G (IgG) examined by immunohistochemical methods. *J. Histochem. Cytochem.* 31:411–416.

37. Pilz, I., E. Schwarz, …, M. Sela. 1980. Effect of cleaving interchain disulfide bridges on the radius of gyration and maximum length of anti-poly(D-alanyl) antibodies before and after reaction with tetraalanine hapten. *Proc. Natl. Acad. Sci. USA.* 77:117–121.

38. Heugen, U., G. Schwaab, …, M. Havenith. 2006. Solute-induced retardation of water dynamics probed directly by terahertz spectroscopy. *Proc. Natl. Acad. Sci. USA.* 103:12301–12306.